Topological angular momentum in electron exchange excitation of a single atom

J. F. Williams, L. Pravica, and S. N. Samarin

ARC Centre of Excellence for Antimatter and Matter Studies Centre for Atomic, Molecular and Surface Physics (CAMSP), School of Physics, M013, University of Western Australia, Perth 6009, Australia

(Received 15 July 2011; published 6 February 2012)

In a single free two-valence-electron atom, the motion of the electron spin is a consequence of quantum statistics and the Pauli exclusion principle. Subsequently, during an electron impact exchange excitation from a $^1S_0\, M_S = 0$ to a $^3S_1\, M_S = 0$ state, the electron spin is "parallel transported" around a closed path with a geometrical Berry phase of π radians creating an aligned exchange spin angular momentum. This alignment is observed via the Stokes parameter P_2 of the photon decay into a ^3P state. The geometric phase is in addition to the dynamic phase. Measurements from zinc and mercury atoms in different laboratories show the effect close to the excitation threshold where there are no competing excitation processes. Similar effects are expected in other atomic and molecular quantum scattering processes where comparable geometrical or topological paths exist. Electron quantum scattering theories use antisymmetrized wave functions but none include this geometrical exchange angular momentum.

DOI: 10.1103/PhysRevA.85.022701 PACS number(s): 34.80.Dp

I. INTRODUCTION

The realization of basic concepts of quantum mechanics has led to the use of electron intrinsic spins as quantum memory elements and polarized photons as quantum information carriers. The advances are frequently underpinned by observations and predictions of tunable geometrical and topological phase transitions between electronic states, particularly in insulating materials, and have inspired learning how to make diverse and complex materials and to control their electronic properties. The idea and uses of topological phase has pervaded many areas of science and it is also a unifying concept of its many profound observational consequences. Its applications are many and varied, for example, in magnetism [1], surface physics [2], topological insulators [3], quantum dot resonance fluorescence [4], cold atoms [5], the quantum Hall effect [6], and magnon dynamics [7]. Recently, Berry recalled [8], instructively, the diversity of fundamental ideas and paths leading to his concept and related geometrical and topological phases. Here we explain our recent observations [9] in terms of a geometric Berry phase [10,11] where, in a free single atom with only two electrons in the outer valence orbits, spin-polarized electron exchange excitation from a singlet $S = 0$, $M_S = 0$ to a triplet $S = 1$, $M_S = 0$ state is described essentially as parallel movement of electron spin around a closed path with an inherent phase change of π radians in the wave function. The process causes alignment rather than polarization of the electron charge cloud. The path in a single atom provides exact quantum phase change calibration in addition to the dynamic scattering phase change. We explain two independent observations of zinc $(3d^{10})\,4s^2$ and mercury $(5d^{10})\,6s^2$ ground-state atoms excited by a spin-polarized electron beam.

Following the formulation of the intrinsic spin of fermions [12], seminal contributions [13–15] expanded the concepts and far-reaching effects of electron spin which underpin our approach. The combination of intrinsic spin and topological phases has progressed from thought experiments [16,17] into three types of measurements, usually to observe a topological phase. Here we do not distinguish between geometric and topological phases. The first type transports two beams of particles in well-separated paths, recombines the beams, and searches for interferences, with or without [18] a simultaneous classical dynamic phase. A second type prepares particles in states $|1\rangle$ and $|2\rangle$, parallel transports them around cyclic paths in some parameter space, and observes frequency shifts of transitions between those states [19,20]. The third type prepares particles in states $a|1\rangle + b|2\rangle$ and transports them along a closed path and observes the polarization of photons from the decay of an excitation process, which we follow here. Broader geometrical considerations concern the ideas of how such phases and their consequences can be detected in, for example, wave vortices [8] and chemical reactions [21]. Generally these types of observations are most clear in particle-scattering experiments with incident spin-polarized particles (and/or spin asymmetrical targets and/or geometries) and when observations are made of asymmetries without which opposing fermion spin effects may cancel. Interwoven in such experiments are the effects of spin-orbit coupling arising from either external or internal origins and which may either enable or confuse their interpretations. Our initial fundamental approach uses a beam of spin-polarized electrons and a beam of single two-valence-electron atoms without external electric and magnetic fields which then cannot be invoked to explain our observations. We chose to explore the electron spin exchange excitation from a "pure" singlet $S = 0$, $M_S = 0$ state to a triplet $S = 1$, $M_S = 0$ state with zero orbital angular momentum in both initial and final states was not expected and where a spin-orbit interaction was not expected. These expectations are discussed later. The scattering conditions were chosen so the dynamic phase was small and accurate optical detection methods could be used to observe angular-momentum changes. This approach, thus, chose a simple excitation process in an atom with two electrons in the valence shell and with the Pauli exclusion principle controlling the symmetry of the eigenfunctions and the motion of the electron spins. The experimental environment was confined to the simplicity and exactness of single atoms in a beam.

The experimental studies with zinc atoms leading to the present paper were reported recently in a brief communication [9] as "unexpected effects," and without explanation, in the spin-polarized excitation $(3d^{10}4s^2)^1S_0 \rightarrow (3d^{10}4s5s)^3S_1$ process. That paper outlined briefly the relevant apparatus and experimental methods from the viewpoint of traditional polarized electron scattering from a beam of zinc atoms, the observations of photon polarizations, and the deductions of Stokes parameters and their comparison with quantum scattering calculations. Subsequently we became aware of the work of Goeke [22] and Goeke *et al.* [37] on the spin-polarized excitation in the similar $(3d^{10}6s^2)^1S_0 \rightarrow (3d^{10}6s7s)^3S_1$ process for mercury atoms which is included here as independent evidence supporting our observations. The present paper provides further details of instruments and techniques, an exhaustive description of measurements made to validate and to establish the experimental certainty, and then interprets the observations of nonzero linear Stokes P_2 parameter data (defined later) in terms of a topological phase.

II. EXPERIMENTAL METHOD

The implementation of our approach rests on the well-known quantum descriptions [23,24] relating the observable intensity of electric dipole radiation emitted in a given direction and in a given state of polarization to expectation values of components of the total electronic angular momentum J of the excited state. An intuitive picture of the dipole radiation and its polarization was developed from an orthogonal right-handed xyz axis coordinate system defined by the incident electron beam momentum vector k_e and electron spin P_e for planar scattering geometry [24,25] as represented in Fig. 1. Briefly, the z axis is defined by the propagation vector k_e of a spin-polarized electron beam and the electron transverse spin locates the y direction such that planar symmetry of scattering is defined. Photons, emitted from an atom located at the origin, are observed along the y axis. The observed photon intensity

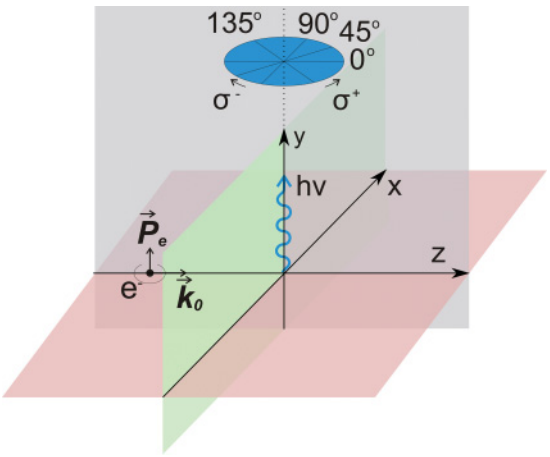

FIG. 1. (Color online) The geometrical (xyz) reference frame and scattering geometry. The spin $\boldsymbol{P_e}$ momentum $\boldsymbol{k_0}$ vectors of the incident electron beam define the scattering (yz) planar symmetry with the target atoms at the origin. Photons emitted along the y axis are analyzed with wavelength filters and linear and circular polarizers before detection with a photomultiplier.

$I(\theta)$ is measured for the linear polarizations parallel to the xz plane with the polarizer transmission axis at an angle θ with respect to the incident electron beam direction and similarly for circular polarization with positive $I(\sigma_+)$ or negative $I(\sigma_-)$ helicities.

The circular polarization of the emitted photons is proportional to the quantum expectation value of the angular momentum of the excited state in the y direction, i.e., the orientation $\langle J_y \rangle$. The linear polarizations are proportional to quantum expectation values of combinations of second-order components of the angular momentum which describe the xz coplanar alignment [25,26] of angular momentum normal to $\langle J_y \rangle$. Quantitative information providing a complete description of the polarization of outgoing photons then is obtained from the Stokes parameters P_i which are defined as $P_1 = [I(0°) - I(90°)]/[I(0°) + I(90°)]$, $P_2 = [I(45°) - I(135°)]/[I(45°) + I(135°)]$, and $P_3 = [I(\sigma_+) - I(\sigma_-)]/[I(\sigma_+) + I(\sigma_-)]$ and from the total intensity which is equal to each of the denominators in those expressions. In that way, those observables can be related [21,22] to physical pictures of the expectation values of components of the total electronic angular momentum J of the excited state and to the orientation and alignment (tensors) of the electron charge cloud of the excited state or equivalently calculated the quantum scattering amplitudes and phases.

The implementation of the corresponding experimental approach has been described previously [9]. Briefly, the polarized electrons arise by photoemission from a GaAs surface by 830-nm circularly polarized light in a UHV system at 4×10^{-11} Torr. Both zinc and mercury atoms have two electrons in their outer shell with energy-level separations providing optical transition with short radiative lifetimes and enabling efficient polarization analyzers for the radiation detected by single pulse counting systems with nanosecond timing resolution. Relatively large cross sections and long particle counting times resulted in good statistical counting accuracy. For both zinc and mercury atoms, excitation from the ground $ns^2\ ^1S_0$ state to the $ns(n+1)s\ ^3S_1$ state, with observation of the decay radiations into the $ns\,np\ ^3P_{J=0,1,2}$ sublevels (with $n = 4$ for zinc and 6 for mercury), is of interest within about 0.5 eV of threshold where there is no cascade radiation and no alternative excitation process. Importantly, the fine-structure states $J = 0,1,2$ for both atoms were well separated. The measurements were made for single atoms in a beam in an electric and magnetic field-free environment.

A. Validity of the techniques

The brief communication [9] of the unexpected results for zinc atoms gave rise to many questions about the experimental details. Here we describe the many tests made to ensure the validity, accuracy, and precision of the techniques and measurements, particularly for the validity of the nonzero values of P_2. These tests are mentioned with far more detail than usually presented because of this first reported interpretation of a topological phase for single atoms and of the associated need to define precisely the observed quantities.

(i) During a 6-year period the whole apparatus was taken apart and moved to a preferred environmental

location. The vacuum chamber was disassembled completely, a nonmagnetic mounting frame installed and the chamber reassembled. The mu-metal shielding and the Helmholz coils were redesigned and optimized to attain a residual mean field of 7 mG, and a magnetic field gradient averaging 7 mG/cm, in the interaction region and space traversed by the electron spin. This procedure checked the validity of procedures of alignment, the precision of construction, and the abilities of the operator to maintain accurate measuring procedures.

(ii) The electron and zinc beams were changed with two different zinc ovens but of the same design and using two different batches of zinc by different manufacturers. The experiments were repeated with at least three different GaAs crystals, with normal crystal 30% polarization, two different types of strained crystals yielding 66% polarization, and unpolarized electron beams. Even the power supplies for all internal components were changed and induced voltages from ground loops, for example, were reduced to below millivolt levels.

(iii) Each of the three transitions was well resolved. The list of filters (and full-width-at-half-maximum transmission) include (a) 468.6 nm (0.9 nm) not tilted and tilted at 4°; (b) 472.4 nm (0.9 nm) and 473.4 nm (1.9 nm) tilted at 6.5°, 472.4 nm (0.87 nm), 473.9 nm (0.8 nm); (c) 481.64 nm (9.7 nm) and 483.8 nm (1.4 nm) tilted at 12°. All precision interference filters were changed and even some other filters were tilted to move their central wavelength to the required wavelengths and then it was shown that tilting had no effect on the polarization. The measurements were unchanged when repeated with an acousto-optic tunable filter (AOTF, Brimrose TEAF7) with a resolution of about 1 nm at those wavelengths.

(iv) The optical detection system and components were changed. Two different liquid crystal variable retarder (LCVR, Medowlark B1020) and linear polarizer (Melles Griot FPC) were replaced. Both LCVRs (source and detector) were recalibrated multiple times. Three different vacuum windows (two visible and one passing UV photons) were used after testing their transmission and stress performances. Two photomultiplier tubes each with their own temperature coolers (from different manufacturers) were used. The data for the $4s5s\ ^3S$ decay radiation clearly indicated polarization at 45° and 135°, corresponding to nonzero P_2, and no polarization at 0° and 90°, corresponding to zero values of P_1.

(v) The electronic detection system including all pulse counting components and the computer acquisition system were replaced. Also P_2 was not affected by measurements using an automated stepper motor for rotation of the linear polarizer rather than the LCVR.

In summary, all changes in the apparatus gave the same nonzero values of P_2, after normalization to the polarization of the electron beam and within the statistical measuring uncertainties of the magnitudes shown in Fig. 2. This extreme and probably unique relocation and reconstruction of the apparatus, replacement of the parts, and obtaining the same results add considerable credibility to the data. We note also our earlier studies of other transitions [27–33] over about 10 years which showed a high precision, accuracy and validity of the measurements and, hence, support the present descriptions.

III. RESULTS

Figures 2 and 3 for zinc [9] and mercury [37] atoms, respectively, show the Stokes parameters for excitation from the ground $ns^2\ ^1S_0$ state to the $ns\,(n+1)s\ ^3S_1$ state, with observation of the decay radiations into the $ns\,np\ ^3P_{J=0,1,2}$ sublevels (with $n=4$ for zinc and 6 for mercury). The zinc data were published recently [9] but are reproduced here because of the need to indicate visually the close behavior of all three Stokes parameters for all three fine-structure states of both zinc and mercury.

The fine-structure states $J = 0,1,2$ for both atoms were well separated. The zinc data show good statistical counting accuracy for the 468.1 nm $J = 0$ data and proportionally for the $J = 1,2$ fine-structure excitations. The mercury data by Goeke show more varied statistical variations but were considered excellent for the 1983 instrumentation and for their intended purpose. The energy region of interest concerns only where a single excitation process is energetically possible, that is, within about 0.5 eV of threshold as indicated by the thin vertical lines, up to the next highest excitation threshold, i.e., there is no cascade radiation and no alternative excitation process.

A large number of facts are clear:

(i) The values of P_2 (second row in both Figs. 2 and 3) and P_3 (third row of Figs. 2 and 3) are nonzero for all three fine-structure transitions for both zinc and mercury.

(ii) The nonzero P_2 values arise only from the use of incident spin-polarized electrons in the excitation process and their associated planar symmetry.

(iii) Data with unpolarized incident electrons (measured only for zinc) indicate with negligible uncertainty that the P_2 parameter for incident unpolarized electrons is zero within the observed values of 0.0005 ± 0.0005. This feature occurs because cylindrical symmetry prevails for unpolarized electrons in a beam.

(iv) For both atoms within the counting statistical uncertainties, the ratios of the P_2 and P_3 Stokes parameters for the three fine-structure $j = 0,1,2$ transition photons, are in the ratios required by the $6j$ angular-momentum coupling coefficients and the state multipoles [24] for well LS-coupled states, i.e., the P_2 values are in the ratios of -1, $1/2$, and $-1/10$ and P_3 values are in the ratios of 1, $1/2$, and $-1/2$, respectively.

(v) These results required separate measurements for P_2 and P_3 for each wavelength and each atom, i.e., the validity of the measurement technique and interpretation have been supported in a total of six measurements for each atom.

(vi) Further, and importantly, while the fine-structure states $J = 0,1,2$ were well separated by optical filters and their spectra were measured at different times, the fact that the P_3 values for the $J = 1$ and 2 states are of opposite sign to each other, and that P_3 for $J = 0$ and $J = 1$ are of opposite sign also, indicates that their signals would subtract and cause P_3 for the $J = 0$ to be much lower than its value of near unity.

(vii) The signs of P_2 and P_3 both changed when the incident electron spin was inverted. Also the measured values changed proportionately with changes in the degree of polarization of the incident electron beam from usually 30 to 66% caused proportional changes in P_2 and P_3.

(viii) Further confirmations of the validity of the measurements are the values of P_1 and P_3, which show the expected and predicted results. If nonzero values of P_2 were caused by some instrumental effect, there is no reason why P_1 and P_3 should not have been affected. Three transitions with different wavelengths were studied and all three exhibit the same behavior. Furthermore, the nonzero P_2 values were evident in three different transitions and their values agreed with the depolarization indicated by the $6j$ symbols.

In summary, these eight considerations indicate strong support for the validity and self-consistency of the measurements.

Additional evidence for the validity and significance of our measurements was obtained from the Stokes parameters for excitation of a neighboring ^1S state where exchange does not occur. Observations of the 518.2-nm decay radiation from the excited $4s6s\,^1S_0$ state to the $4p\,^1P$ state are shown in Fig. 4. Within about the first 0.6 eV above the 8.19-eV threshold for excitation all three integrated Stokes parameters are zero within the statistical uncertainties. This result is consistent with the absence, at least below detection levels, of exchange excitation for a well LS-coupled singlet state with a spherical electron charge cloud. Both P_2 and P_3 are negligibly small compared with the data for the $5s^3S$ excitation. The data are also consistent with the expectation that Mott scattering is not likely to be effective for the S-state excitation without exchange. In summary, our apparatus and techniques measured zero Stokes parameters for a ^1S state where zero should be measured where both exchange and Mott scattering are expected to be zero. About 1 eV above threshold the three P_i parameters are definitely nonzero, most likely by transfer of polarization through cascade from higher states, but the possibility of resonance phenomena cannot be excluded for an electron energy resolution of about 0.3 eV; however, it is only the threshold region that is of concern here.

IV. EXCHANGE AND SPIN-ORBIT EFFECTS IN MERCURY

The results from the zinc studies alone are sufficient and necessary to justify our interpretation in the next section. However, the marked similarity of behavior between all of the above data for zinc and mercury requires the following comments. The common factors are the exchange excitation process from a ^1S to a ^3S state, the electronic structure of two electrons in the outer valence shell, and that the P_3 values of the fine-structure levels are in the ratio of 1, $\frac{1}{2}$, and -1/2 and P_2 values in the ratio required by the Clebsch-Gordan coefficients of -1, $1/2$, and $1/1$, the third value not being determined with sufficient certainty. Moreover, the energy resolutions of the mercury and zinc data are similar, which assists their visual comparison.

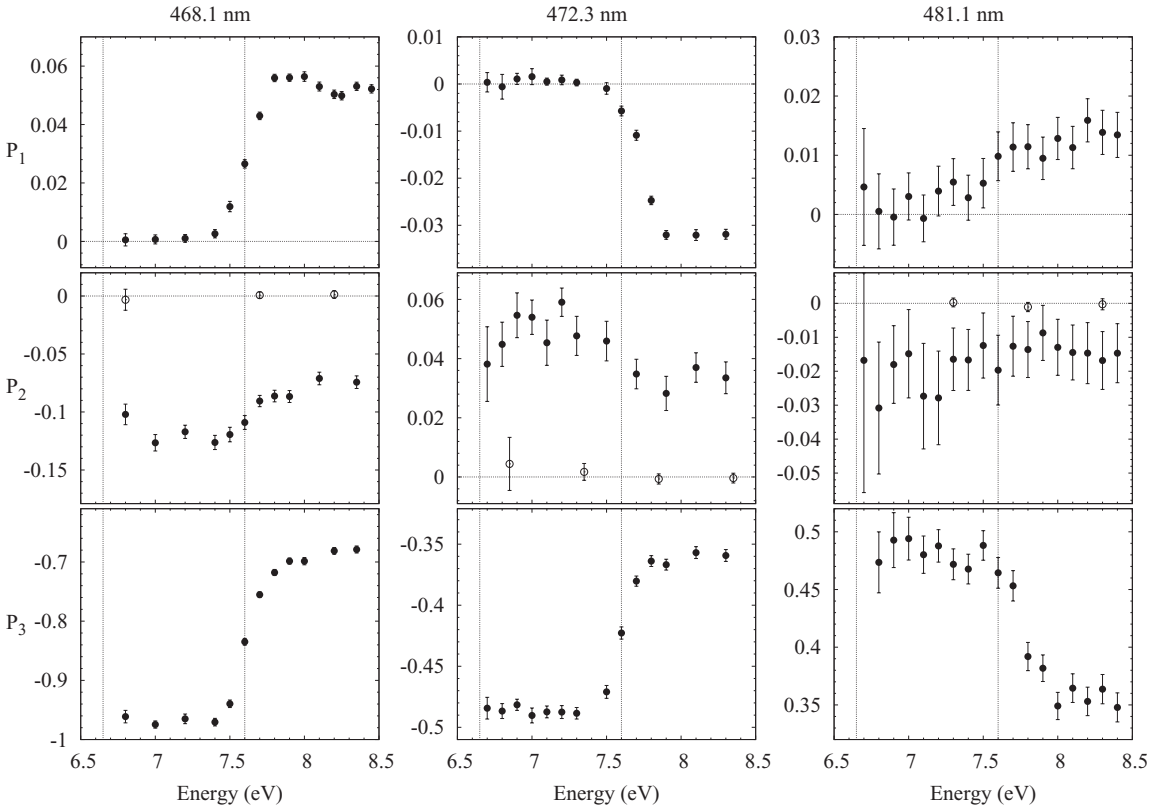

FIG. 2. The integrated Stokes parameters $P_{i=1,2,3}$ for zinc atoms excited from the ground $4s^1S_0$ state to the $5s^3S_1$ state and observed by the subsequent radiative decay to the $4p\,^3P_{0,1,2}$ states with photon wavelengths for $J = 0,1,2$ of 468.1, 472.3, and 481.1 nm, respectively. The data were normalized to an electron beam polarization which varied for different measurements but was normally of the order of $66 \pm 0.5\%$. The threshold excitation energy for the $4s5s\,^3S_1$ state is 6.65 eV and for the first cascading $5p\,^3P$ state at 7.6 eV, as shown by the vertical lines. The open circles indicate measurements using unpolarized electrons and the closed circles using polarized incident electrons and normalized to the average incident spin P_{e^-}.

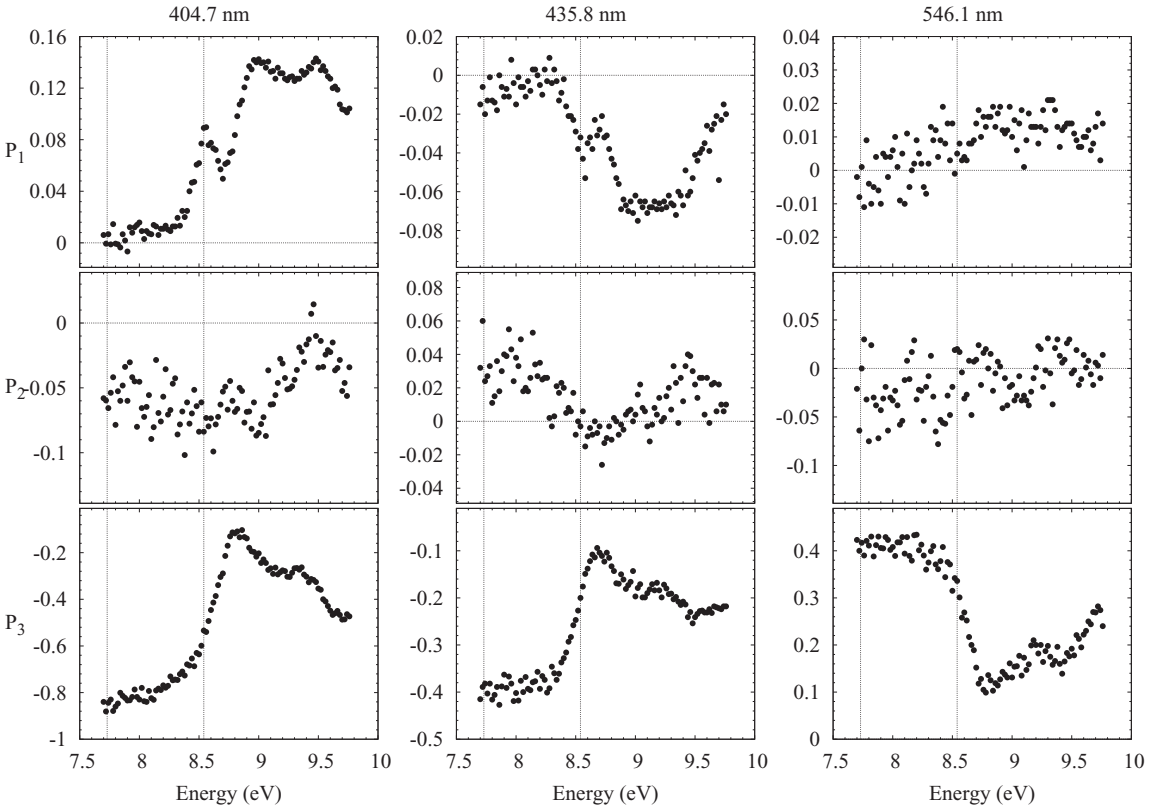

FIG. 3. The integrated Stokes parameters $P_{i=1,2,3}$ for mercury atoms excited from the ground $6s^1S_0$ state to the $7s^3S_1$ state and observed by the subsequent radiative decay to the $6p^3P_{0,1,2}$ states with photon transition wavelengths for $J = 0,1,2$ of 404.7, 435.8, and 546.1 nm respectively. The data were normalized to an electron beam polarization which varied from plot to plot from 24% to 32%. The threshold excitation energy for the $6s7s^3S_1$ state is 7.71 eV and for the first cascading $7p^3P$ state at 8.60 eV, as shown by the vertical lines. The original data of Goeke have been transposed from Stokes "eta" to P parameters (see text).

It is known [26,34–36] that an incident unpolarized low-energy electron beam scattered elastically from the $(6s^2)^1S_0$ ground state of mercury may be spin polarized due to the spin-orbit interaction. It is possible that a similar polarization change may occur during exchange excitation of the $7s^3S_1$ state and its occurrence concurrently with a nonzero P_2 may present an interpretation other than that offered below but an alternative explanation is probable. Observations of the nearby $6s6p^3P_1$ state [22] are described well with calculated "intermediate coupling" with the total orbital angular momentum ($L = 1$) a reasonably good quantum number while the total spin ($S = 1$) requires a singlet admixture such that all three light polarizations are nonzero. Exchange is necessary for excitation of the ^3P state and gives rise to a nonzero P_3; however, the P_1 Stokes parameter is zero, which suggests that the consequences of intermediate coupling are minimal here because the $6s6p^3P_1$ state is not involved in the near-threshold region of our observations and contributes only via cascading angular momenta from the spin-exchanged $7s^3S_1$ state. Second, the behavior of the observed P_i for mercury with energy is consistent with our data for zinc.

A feature of the measurements for mercury is that they were made by Goeke in 1983 in Germany [37] as part of unpublished Ph.D. studies. However, Goeke published [22] only the Stokes parameters P_1 and P_3 as evidence of the effects of electron exchange from a ^1S to a ^3S state while the P_2 data were discussed only above about 8.8 eV and not for the threshold region of prime interest here and then only as indicating spin-orbit interaction near the excited resonance state of the negative mercury ion. Also the interpretations of the Goeke data in general concerned only the energy region above that of interest here. Note that the original data of Goeke [37] used an equivalent "eta" parameter sign convention for the Stokes parameters and that data have been adapted to the sign convention used here.

V. INTERPRETATION OF THE STOKES PARAMETERS

To explain our results we indicate, explicitly, (i) how electron spin exchange within an excitation process and within a single atom produces spin rotation and, hence, an effective spin-orbit interaction; (ii) how the resultant phase change of fermions appears, without modification, in an observable such as alignment of an excited electron charge cloud; (iii) how the Bartschat and Blum model remains an effective angular momentum model; and (iv) why a geometrical Berry phase change of π radians is a viable and most probable interpretation.

The essential physical insight of Berry and Robbins [11] was the realization that the phase change of π radians, which was required for the electron exchange excitation from the combination of spin functions of the ground $M_S = 0$ singlet

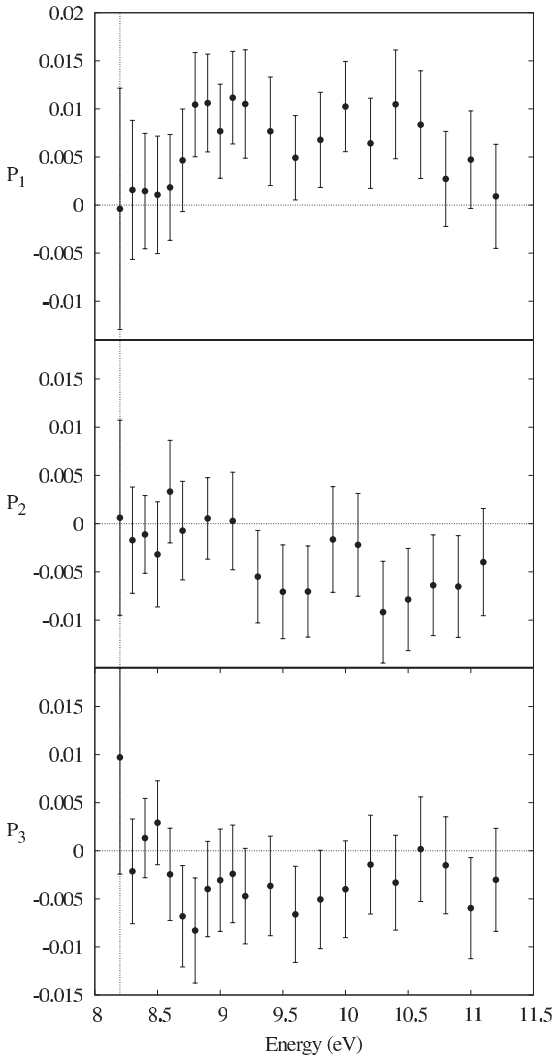

FIG. 4. The Stokes parameters $P_{1,2,3}$ of the 518.2-nm decay radiation to the $4p^1P$ state following excitation from the ground $4s^2\,{}^1S_0$ state to the $6s\,{}^1S$ state.

to those of the excited $M_S = 0$ triplet state, occurred by a rotation of $\pi/2$ rad of each single spin and that was equivalent to a π rad rotation of a two-particle spinor. Also the concept of parallel transporting a single electron spin around a geometrically closed path removed the possibility of an external force changing the direction of the spin and so leaving only electron exchange as the mechanism of spin change and, hence, an effective exchange angular momentum. Two models, albeit elementary, are given to assist the visualization of the electron exchange phase change of π radians. First, a simple semiclassical vector model, as in Fig. 5, affords a simple representation and visualization of the singlet and triplet spin functions of a two-electron spin and their quantum phases.

Let **u** (up) and **d** (down) represent the spin states and 1 and 2 represent the electrons. The singlet ground-state asymmetric spin function ($\mathbf{u}1\cdot\mathbf{d}2$-$\mathbf{d}1\cdot\mathbf{u}2$) for the $S = 0$, $M_s = 0$ state is represented by the two-electron $\mathbf{u}1\cdot\mathbf{d}2$ spin vector (pointing down) and by $\mathbf{d}1\cdot\mathbf{u}2$ (pointing up, shown dotted) such that their relative phase is π radians and their projections onto the vertical (quantization) axis cancel to give $M_s = 0$. It is implicit

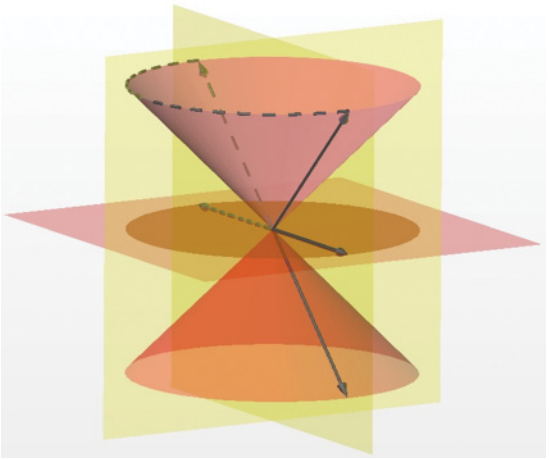

FIG. 5. (Color online) Vector representation of the ${}^1S\,M_S = 0$ (dashed lines) and ${}^3S\,M_S = 0$ (solid line) spin angular momenta and phases. The vertical quantization y axis is normal to the xz plane in which the π rad geometric phase is represented, as defined in Fig. 1.

that the spins are rotating randomly but when observed with a given quantization direction, here the y axis, they may be represented as shown, and for fermion spin $1/2$ only multiples of π rad are quantum allowed changes. Moreover, the direction of rotation changes for opposite spins of the incident electron. Then let the electron exchange mechanism effectively rotate the $\mathbf{d}1\cdot\mathbf{u}2$ vector by $+\pi$ radians such that the three vectors on the right-hand side indicate the triplet state symmetric spin function ($\mathbf{u}1\cdot\mathbf{d}2 + \mathbf{d}1\cdot\mathbf{u}2$) for $S = 1$ in such a way that their sum leaves only the horizontal (xz plane) vector with projection on the vertical axis representing $M_s = 0$ for $S = 1$. The $M_S = \pm 1$ symmetric spin functions, $\mathbf{d}1\cdot\mathbf{d}2$ and $\mathbf{u}1\cdot\mathbf{u}2$, are not shown as they do not offer a parallel (closed) degenerate phase path in the excitation process and are not of further interest here.

Figure 6 shows the second model indicating parallel transport around the closed path shown by a full blue (yellow) line encompassing a quarter sphere with a solid angle of π radians for spin up (down). Parallel transport [10,11] of a spin

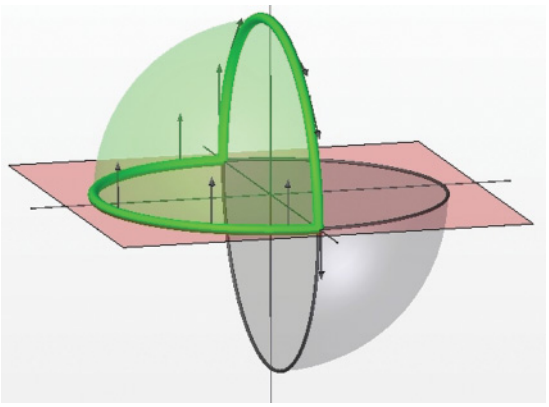

FIG. 6. (Color online) Parallel transport, around a closed path of π rad. The top left (green) section shows the parallel transport of the spin vector, starting at nearest end of equatorial diameter with spin up and ending with spin down after exchange. The lower right (gray) section indicates the path for the opposite incident spin. The vertical axis is the quantization direction.

vector $|s(r)\rangle$ around a surface means that the length of $|s(r)\rangle$ is unchanged, that $\langle s(r)|s(r)\rangle$ is unchanged for all r, and that $|s(r)\rangle$ and $|s(r+dr)\rangle$ have the same phase. When the path is closed, $|s(r)\rangle = \exp(i\phi)\,|s(r)\rangle$, where ϕ is the geometric spin phase of π radians. The total phase is then the sum of ϕ and the dynamic phase obtained from solutions of the Hamiltonian which gives the normal energy eigenstates. In that way a single spin of either direction will cause a phase change of π radians as shown by experiment and an unpolarized electron beam with an average of equal numbers of spin up and spin down has equal and opposite effects, i.e., no change. However, for a polarized incident electron, the two electron target atom spin is parallel transported around an equatorial plane and then exchanged "in the vertical plane" to arrive back at the starting point with a phase change of π radians.

Given the statistical combinations of the spin functions for both the initial and final $M_S = 0$ states and the insight of Berry and Robbins, the above exchange phase models are consistent with the Bartschat and Blum model [25] in which the electron change cloud becomes aligned but not polarized. The expectation values of angular momenta $\langle S_x S_z + S_z S_x\rangle$ (appropriately normalized) are represented by the xz-planar vector components of Fig. 5 and are also proportional to the P_2 parameter. The observations of nonzero P_3 Stokes parameter are also consistent with a nonzero $\langle S_y\rangle$ i.e., spin angular momentum normal to the scattering xz plane.

Implicit in the radiative decay of the triplet state, this exchange angular momentum (carrying phase and rotation) is coupled to the angular momentum of an oscillator of the excited quantum electrodynamic field [14] to an emergent photon (boson) satisfying energy and momentum conservation for the radiative decay. The observed polarization of the emitted photon and the observational technique become apparent using a Poincare-type sphere to describe the rotation of electron spin in its phase space and the rotation of photon angular momentum in coordinate space. The phase coherence is preserved from the time of exchange ($\sim 10^{-15}$ s) until the emitted photon is observed, i.e., when the wave function "collapses" after about $\sim 10^{-8}$ s.

Finally, a summary of the theoretical scattering models and references for electron exchange excitation for zinc [29], [38] and mercury [39,40] atoms have been given recently. For example, in zinc both valence $3d^{10}4s,4p,4d,5s\ P(nl)$ orbitals, and core-valence $3d^9 4s^2\ P(nl)$ electron correlations were included for target-state description. The best quantum scattering calculations, both perturbative and nonperturbative, including the R-matrix, CCC, and relativistic distorted-wave calculations, with all their nuances, were used. All approaches have found that P_1 and P_2 are essentially zero near threshold and that P_3 values (normalized to the incident electron beam polarizations) are in the ratios of -1, -0.5, and 0.5 for the $J = 0$, 1, and 2 fine-structure levels and in good agreement with observations for the P_1 and P_3 Stokes parameters.

The assumptions of Bartschat and Blum for the dynamics of the process that spin-orbit interaction, for the projectile and the representation of the target state, are negligibly small and that the excitation is a nearly pure spin-exchange excitation process have been supported by all models used for calculations. In contrast, the measurements here indicate an effective spin-orbit contribution. The well-established model of Bartschat and Blum remains valid if the nonzero P_2 values are interpreted as consequences of the rotational motion of the exchanged electron spin causing an effective angular momentum and associated spin-orbit interaction. The origin is, thus, a target structural, and not a continuum electron, spin-orbit interaction; The latter, if present, would appear in the ^1S excitation. The task remains for theory to include a topological nondynamical phase.

VI. DISCUSSION AND OUTLOOK

A geometric phase has been shown for exchange excitation in zinc and mercury atoms with two electrons in the outer shell and in angular momentum $M_S = 0$ states with initial and final states of odd multiplicities, i.e., with spin degeneracies. The effect can be expected for all excitation-with-exchange process wherever the initial and final states present a closed loop path for parallel electron spin transport. Other single atoms, with higher spin multiplicities, are expected to show topological effects where the exchange topological phase has values of $(-1)^{2S}$ noninteger S values. We did not attempt to measure P_2 for the similar 1^1S_0 to 3^3S_1 excitation process via its radiative decay to the 2^3P state in helium because we could not resolve optically, with polarization analysis, the 0.2-nm separated final m_J states and obtain acceptable counting statistical accuracy. Atomic hydrogen, being a single electron atom, would not show a topological phase of similar origin while the negative hydrogen ion H^- and positronium may show such phase.

As pointed out by Berry and Robbins [11], there is no preferred quantization axis for the observation of this topological effect, otherwise one component of the spin may not be exchanged. This result paves the way for other observational modes of topological effects such as for incident unpolarized electron scattering when cylindrical symmetry is broken and planar symmetry exists, for example, via the detection in coincidence of two or more outgoing particles [26]. Electron impact ionization scattering can be expected to show a topological phase effects [31], for example, for $(e,2e)$ coincidence studies, particularly for the energies and angles preferred by spin degeneracies. Positronium scattering, molecular excitation, and dissociation, for example, are expected to show similar topological effects. The notion of an effective magnetic monopole [41] is also consistent with the observations and occasionally useful in discussion.

It is the Fermi statistics, and then the Pauli exclusion principle, which create the topological path. For an atom with two electrons in the valence shell with degenerate spin functions, the exchanged spins are parallel transported along a topological closed-loop path with a fixed phase of π radians. The associated exchange spin angular momentum has been observed as a coherent alignment of the excited electron charge cloud.

ACKNOWLEDGMENTS

The research was supported by the Australian Research Council and the University of Western Australia. The expertise of G. Light and S. Key in the mechanical workshop of the University made the studies possible. Data from Goeke's 1983 thesis were forwarded with permission to use by F. Hanne, University of Muenster. Discussions with K. Bartschat, O. Zatsarinny, and A. D. Stauffer are appreciated.

[1] P. M. Haney and M. D. Stiles, Phys. Rev. Lett. **105**, 126602 (2010).
[2] Xiao-Liang Qi *et al.*, Science **323**, 1184 (2009).
[3] M. Z. Hasan and C. L. Kane, Rev. Mod. Phys. **82**, 3045 (2010).
[4] A. N. Vamivakas *et al.*, Nature **467**, 297 (2010).
[5] Y. J. Lin, K. Jimenez-Garcıa, and I. B. Spielman, Nature **471**, 83 (2011).
[6] Y. K. Kato *et al.*, Science **306**, 1910 (2004).
[7] B. Nafridi, T. Keller, H. Manaka, A. Zheluder, and B. Keimer, Phys. Rev. Lett. **106**, 177202 (2011).
[8] M. V. Berry, Nat. Phys. **6**, 148 (2010).
[9] L. Pravica, J. F. Williams, D. Cvejanovic, S. Samarin, K. Bartschat, O. Zatsarinny, A. D. Stauffer, and R. Srivastava, Phys. Rev. A **83**, 040701(R) (2011).
[10] M. V. Berry, Proc. R. Soc. London A **392**, 45 (1984).
[11] M. V. Berry and J. M. Robins, Proc. R. Soc. London A **453**, 1771 (1997).
[12] P. A. M. Dirac, Proc. R. Soc. A **117**, 610 (1928).
[13] W. Pauli, Phys. Rev. **58**, 716 (1940).
[14] J. Schwinger, *Quantum Theory of Angular Momentum*, edited by L. C. Biedenharn and H. Van Dam (Academic Press, New York, 1965), p. 222.
[15] R. P. Feynman, *The 1986 Dirac Memorial Lectures*, edited by R. P. Feynman and S. Weinberg (Cambridge University Press, Cambridge, UK, 1987).
[16] H. J. Bernstein, Nature **315**, 41 (1985).
[17] Y. Aharanov and L. Susskind, Phys Rev. **158**, 1237 (1967).
[18] A. Ioffe and F. Mezei, Physica B **297**, 303 (2001).
[19] Y. Aharonov and J. Anandan, Phys. Rev. Lett. **58**, 1593 (1987).
[20] J. Anandan and Y. Aharonov, Phys. Rev. Lett. **65**, 1697 (1990).
[21] D. C. Clary, Science **309**, 1195 (2005).
[22] J. Goeke, G. F. Hanne, J. Kessler, and A. Wolcke, Phys. Rev. Lett. **51**, 2273 (1983).
[23] J. Macek and D. H. Jaecks, Phys. Rev. A **4**, 2288 (1971).
[24] U. Fano and J. Macek, Rev. Mod. Phys. **45**, 553 (1973).
[25] K. Bartschat and K. Blum, Z. Phys. A **304**, 85 (1982).
[26] N. Andersen and K. Bartschat, *Polarization, Alignment, and Orientation in Atomic Collisions* (Springer, New York, 2001).
[27] S. A. Napier, D. Cvejanovic, J. F. Williams, and L. Pravica, Phys. Rev. A **81**, 032701 (2010).
[28] S. A. Napier, D. Cvejanovic, J. F. Williams, L. Pravica, D. Fursa, I. Bray, O. Zatsarinny, and K. Bartschat, Phys. Rev. A **79**, 042702 (2009).
[29] S. A. Napier, D. Cvejanovic, J. F. Williams, and L. Pravica, Phys. Rev. A **78**, 032706 (2008).
[30] L. Pravica, J. F. Williams, D. Cvejanovic, and S. A. Napier, Phys. Rev. A **75**, 012721 (2007).
[31] J. F. Williams and D. H. Yu, Phys. Rev. Lett. **93**, 073201 (2004).
[32] J. F. Williams, D. Cvejanovic, S. Samarin, L. Pravica, S. A. Napier, and A. D. Sergeant, J. Phys. Conf. Ser. **80**, 012023 (2007).
[33] J. F. Williams, L. Pravica, D. Cvejanovic, S. A. Napier, S. Samarin and M. Piwinski, J. Phys. Conf Ser. **235**, 012005 (2010).
[34] G. F. Hanne and J. Kessler, J. Phys. B **9**, 791 (1976).
[35] G. F. Hanne, J. Phys. B **9**, 805 (1976).
[36] N. Andersen, J. W. Gallagher, and I. V. Hertel, Phys. Rep. **165**, 1 (1988).
[37] J. Goeke, Ph.D. thesis, University of Meunster, Germany (1983).
[38] L. Pravica, Ph.D. thesis, University of Western Australia (2006).
[39] O. Zatsarinny and K. Bartschat, Phys. Rev. A **71**, 022716 (2005).
[40] O. Zatsarinny and K. Bartschat, Phys. Rev. A **79**, 042713 (2009).
[41] R. Bhandari, Phys. Rep. **281**, l (1997).